Original Article

Functional-structural large-scale brain networks are correlated with neurocognitive impairment in acute mild traumatic brain injury

Yin Liu[1#], Fengfang Li[1#], Song'an Shang[1], Peng Wang[1], Xindao Yin[1], Vijaya Prakash Krishnan Muthaiah[2], Liyan Lu[1], Yu-Chen Chen[1]

[1]Department of Radiology, Nanjing First Hospital, Nanjing Medical University, Nanjing, China; [2]Department of Rehabilitation Sciences, School of Public Health and Health Professions, State University of New York at Buffalo, Buffalo, NY, USA

Contributions: (I) Conception and design: L Lu; (II) Administrative support: YC Chen; (III) Provision of study materials or patients: Y Liu, F Li; (IV) Collection and assembly of data: Y Liu, P Wang; (V) Data analysis and interpretation: L Lu, S Shang, X Yin, VP Krishnan Muthaiah; (VI) Manuscript writing: All authors; (VII) Final approval of manuscript: All authors.

[#]These authors have contributed equally to this work.

Correspondence to: Liyan Lu, MD, PhD; Yu-Chen Chen, MD, PhD. Department of Radiology, Nanjing First Hospital, Nanjing Medical University, No. 68, Changle Road, Nanjing 210006, China. Email: luliyan.ok@163.com; cycxwq@njmu.edu.cn.

Background: This study was conducted to investigate topological changes in large-scale functional connectivity (FC) and structural connectivity (SC) networks in acute mild traumatic brain injury (mTBI) and determine their potential relevance to cognitive impairment.

Methods: Seventy-one patients with acute mTBI (29 males, 42 females, mean age 43.54 years) from Nanjing First Hospital and 57 matched healthy controls (HC) (33 males, 24 females, mean age 46.16 years) from the local community were recruited in this prospective study. Resting-state functional magnetic resonance imaging (rs-fMRI) and diffusion tensor imaging (DTI) were acquired within 14 days (mean 3.29 days) after the onset of mTBI. Then, large-scale FC and SC networks with 116 regions from the automated anatomical labeling (AAL) brain atlas were constructed. Graph theory analysis was used to analyze global and nodal metrics. Finally, correlations were assessed between topological properties and neurocognitive performances evaluated by the Montreal Cognitive Assessment (MoCA). Bonferroni correction was performed out for multiple comparisons in all involved analyses.

Results: Compared with HC, acute mTBI patients had a higher normalized clustering coefficient (γ) for FC (Cohen's d=4.076), and higher γ and small worldness (σ) for SC (Cohen's d=0.390 and Cohen's d=0.395). The mTBI group showed aberrant nodal degree (Dc), nodal efficiency (Ne), and nodal local efficiency (Nloc) for FC and aberrant Dc, nodal betweenness (Bc), nodal clustering coefficient (NCp) and Ne for SC mainly in the frontal and temporal, cerebellum, and subcortical areas. Acute mTBI patients also had higher functional-structural coupling strength at both the group and individual levels (Cohen's d=0.415). These aberrant global and nodal topological properties at functional and structural levels were associated with attention, orientation, memory, and naming performances (all $P<0.05$).

Conclusions: Our findings suggested that large-scale FC and SC network changes, higher correlation between FC and SC and cognitive impairment can be detected in the acute stage of mTBI. These network aberrances may be a compensatory mechanism for cognitive impairment in acute mTBI patients.

Keywords: Graph theory analysis; resting-state functional MRI; diffusion tensor imaging (DTI); mild traumatic brain injury (mTBI); cognitive decline

Submitted May 04, 2022. Accepted for publication Nov 07, 2022. Published online Nov 29, 2022.
doi: 10.21037/qims-22-450
View this article at: https://dx.doi.org/10.21037/qims-22-450

Introduction

The burden of global neurotrauma has been on the rise (1). Approximately 50 million traumatic brain injuries (TBIs) occur throughout the world every year (2), of which 80–90% are classified as mild TBI (mTBI) (3). MTBI is associated with neurocognitive dysfunction at the acute stage, and more than 20% of cases continue to report long-term neurocognitive complications years after the injury (4). With the rising prevalence of mTBI, cognitive problems followed by mTBI have attracted increasing attention (5-7). However, in the acute stage, mTBI patients with cognitive impairment lack brain abnormalities on conventional imaging modalities. Thus, the neurobiological mechanism of post-mTBI cognitive impairment is not fully understood.

In recent years, aberrant functional and structural networks have been detected in disease conditions including epilepsy (8), stroke (9), Parkinson's disease (10), and Alzheimer's disease (11). Moreover, the graph theory approach has emerged as a promising technique for characterizing functional and structural networks in a complex network at global and nodal levels (12). In the context of this approach, the human brain is modeled as a complex large-scale network that consists of substantial connecting nodes and edges. Meanwhile, a number of topological properties have been evaluated using the graph theory analysis. Some frequently used topological properties, such as global network properties (clustering coefficient and characteristic path length) and nodal properties [nodal degree centrality, nodal betweenness centrality and nodal efficiency (Ne)], have been reported to provide valuable insights into possible mechanisms underlying cognitive impairments in various neurological diseases.

To date, only a few studies have applied the graph theory approach to describe topological characteristics for functional connectivity (FC) and structural connectivity (SC) in mTBI. Patterns of FC and SC can be investigated using resting-state functional magnetic resonance imaging (rs-fMRI) and diffusion tensor imaging (DTI), respectively. Previous rs-fMRI and DTI findings revealed that mTBI patients had aberrant topological features that reflect disrupted modular organization, functional small world property changes, and diffuse axonal injury. These aberrances were related to depression scores or post-concussion symptom scale (PCSS) scores (12-15). However, many of these mTBI studies used either rs-fMRI for FC analysis or DTI for SC analysis or were conducted during the subacute and chronic stages of recovery. Although one DTI study demonstrated SC abnormalities using graph theoretical analysis in acute mTBI, the population was children not adults. More importantly, FC and SC are interdependent. Their combination could detect subtle brain changes more sensitively than any single imaging modality (8,16) and contribute to a better understanding of brain connectivity alterations (17). Previous literature has demonstrated abnormal FC-SC relationships in bipolar disorder (18), idiopathic generalized epilepsy (8), and diabetic kidney disease (19). Only a single study reported an aberrant relationship between FC and SC in acute mTBI, but it did not explore the correlation between the FC-SC relationship and neurocognitive performance (20). Therefore, integrating the information from structural and functional networks could help unveil the neurobiological mechanism of cognitive impairment following acute mTBI and remains to be studied.

We hypothesized that brain functional and structural large-scale network organization would differ significantly between mTBI patients during the acute stage of injury and healthy control (HC) participants and that these network alterations would be the partial mechanisms underlying neurocognitive impairments. Therefore, we identified altered large-scale functional and structural brain networks and internship patterns in acute mTBI patients compared with HC. We also investigated the associations between these network alterations and neurocognitive performance. We present the following article in accordance with the STROBE reporting checklist (available at https://qims.amegroups.com/article/view/10.21037/qims-22-450/rc).

Methods

Participants

This study is a prospective study. The study was conducted in accordance with the Declaration of Helsinki (as revised in 2013). The study was approved by the Institutional Review Board of Nanjing Medical University. Written informed consent was obtained from all participants before

their participation in the study protocol. The sample size calculation was determined by the freely downloadable software named "PS: Power and Sample Size Calculation" (by William D. Dupont and Walton D. Plummer, Jr). Between April 2019 and January 2020, mTBI patients were recruited from the emergency department of Nanjing First Hospital, and HC participants were recruited from the local community. The inclusion criteria for the mTBI patients were as follows (21): (I) Glasgow Coma Scale (GCS) score ranging from 13 to 15 on presentation to the emergency department and (II) a closed head injury within 14 days with either loss of consciousness (LOC) of shorter than 30 min or posttraumatic amnesia (PTA) of shorter than 24 h. LOC is a disruption of consciousness (22). PTA has been said to terminate with the return of continuous memory for ongoing events (23). The exclusion criteria for all participants (mTBI patients and HC patients) were as follows (21): (I) a history of brain injury; (II) a history of neurological disease and long-standing psychiatric condition; (III) MRI contraindications; and (IV) coexisting alcohol and drug abuse. Furthermore, all participants underwent the neuropsychological assessment via the Beijing version of the Montreal Cognitive Assessment (MoCA) within 24 h after MRI, one of the tools suggested to assess cognitive impairment following mTBI (24). MoCA changes could be not only statistically significant but also clinically relevant from a clinical perspective, even if this screening tool is simple. It appears to be sufficiently stable and sensitive for detecting the early presence of cognitive impairment after mTBI and assess changes over time (24). The MoCA scores contained seven subscales, including the visual-executive index score (MoCA-VEIS), naming index score (MoCA-NIS), attention index score (MoCA-AtIS), language index score (MoCA-LIS), abstraction index score (MoCA-AbIS), memory index score (MoCA-MIS) and orientation index score (MoCA-OIS).

Imaging acquisition

A 3.0 T magnetic resonance imaging scanner (Ingenia, Philips Medical Systems, Netherlands) equipped with a 12-channel head coil was used. Parallel imaging was employed. MRI were performed by two radiographers (5-year experienced and 7-year experienced, respectively) following the same scanning parameters. For each participant, rs-fMRI data, DTI data, and high-resolution T1-weighted anatomic imaging data were acquired. Rs-fMRI data were obtained using a gradient echo-planar imaging sequence [axial: repetition time (TR) =2,000 ms; echo time (TE) =30 ms; slices =36; thickness =4 mm; gap =0 mm; field of view (FOV) =240 mm × 240 mm; acquisition matrix = 64×64; flip angle (FA) =90°, and total volume =230]. The fMRI sequence took 8 min and 8 s. High-resolution T1-weighted anatomic imaging data were acquired with a three-dimensional turbo fast echo (3D-TFE) T1WI sequence [sagittal: TR =8.1 ms; TE =3.7 ms; FA =8°; FOV = 256 mm × 256 mm; acquisition matrix =256×256; thickness =1 mm; gap =0 mm; and total =172 slices]. The fluid-attenuated inversion recovery (FLAIR) employed TR =7,000 ms; TE =120 ms; slices =18; thickness =6 mm; gap =1.3 mm; FA =110°; and voxel size =0.65 mm × 0.95 mm × 6 mm. Susceptibility-weighted imaging (SWI) was obtained with a 3D gradient echo (GRE) sequence: TR =22 ms; TE =34 ms; FA =20°; acquisition matrix =276×319; thickness =1 mm; and FOV = 220 mm × 220 mm. DTI employed the following parameters: TR =3,000 ms; TE =1,000 ms; slices =55; thickness =2.5 mm; gap =0; FA =90°; acquisition matrix =120×177; and FOV =240 mm × 240 mm; 32 volumes with diffusion gradients along 32 nonlinear directions [b=1,000 s/mm^2] and 1 volume without diffusion weighting [b=0 s/mm^2]. The DTI sequence took 11 min and 9 s. All participants were instructed to stay awake and keep their head still. Foam padding was used to reduce head motion (8,21). No participants reported falling asleep during the scanning when asked right after the scanning (8,21).

Image preprocessing

The rs-fMRI data were preprocessed using Graph Theoretical Network Analysis (GRETNA) software (http//www.nitrc.org/projects/gretna) implemented in MATLAB (version R2013b) (25). Standard preprocessing methods were used (8,19,20). First, the first ten volumes were discarded due to the instability of the initial magnetic field. Second, slice time correction was performed to correct the remaining functional images, and head motion was corrected. No group differences were observed with respect to head motion (P>0.05). Then, functional images were spatially coregistered with their high-resolution T1-weighted anatomic images with a voxel size of 3×3×3 mm^3 (25). Next, rs-fMRI time series were bandpass filtered (0.01–0.08 Hz) to improve the signal-to-noise ratio (8) and images were detrended for making strong instrumental stability. In this study, to avoid artificial local spatial correlations, no spatial smoothing was applied (26). To remove spurious sources of variance, the Friston 24 parameter obtained via head

motion correction and signals from cerebrospinal fluid and white matter were regressed. Global brain signals were not regressed in order to result in fewer negative values of brain connectivity (25).

The DTI data were preprocessed using PANDA software (27). PANDA is a MATLAB toolbox for pipeline processing of diffusion MRI images based on the Diffusion Toolkit (http//www.trackvis.org/dtk/) and the FSL tool. First, DICOM files were converted into NIfTI format and the raw images were cropped. Second, the eddy current distortions and head motions were corrected by aligning all 32 noncolinear diffusion-weighted images with the b0 image using an affine transformation. Then, the fractional anisotropy (FA) of each voxel was calculated, and the affine transformation was used to coregister the FA image with the corresponding T1 image in the native space. After that, deterministic white matter tractography based on the fiber assignment by continuous tracking (FACT) algorithm was used in the reconstruction of fibers for each individual DTI dataset (18,28). Continuous fiber tracking was terminated when FA <0.15 or the minimum turning angle >45°.

Quality assurance

Our final analysis was restricted to the participants whose data quality was reliable within a tolerable range (13). Visual inspection at each step was employed to guarantee the quality of the preprocessed rs-fMRI and DTI data (13). After that, a subset of participants' data was removed from the study for the following reasons (13): (I) the functional images did not fall within the prescribed FOV, (II) intensity variation artifacts of low spatial frequency, (III) substantial susceptibility artifacts in inferior frontal and inferior temporal regions, (IV) motion correction failure due to a large amount of abrupt motion (translation >2.0 mm or rotation parameters in any direction >2.0°), and (V) lack of complete imaging frames.

Functional and structural network construction

A total of 116 non-overlapping anatomical regions were defined as the nodes of the functional and structural networks (90 nodes in the non-cerebellar brain: 45 nodes in each hemisphere and 26 nodes in the cerebellum). The 116 brain nodes initially parcellated in MNI space based on the automated anatomical labeling (AAL) atlas were inversely warped back to participants' native space (18). In native diffusion space, these 116 nodes were used as masks to guide the counting of white matter streamlines. If there were at least two streamline counts and the length of passing fibers was longer than 10 mm, any two nodes were considered structurally connected through an edge (18). For each edge, we computed the mean FA values of all fibers as its weights (18). Thus, a 116×116 SC matrix for each participant was constructed with the mean FA values between every paired node. To obtain the FC network, the mean fMRI time series were extracted from all voxels for each of the aforementioned 116 nodes. Then, a 116×116 FC matrix for each participant was determined by computing Pearson's correlation coefficients between the processed time series of every paired node (*Figure 1*).

Graph theory analysis

The graph theoretical properties of large-scale functional and structural networks were calculated using the GRETNA toolbox (29). Network topologic properties included small-world parameters: clustering coefficient (Cp), which quantifies the extent of local interconnectivity or cliquishness of a network, reflecting the global efficiency of a network; characteristic path length (Lp), which measures the extent of overall communication efficiency of a network, reflecting the regional efficiency of a network; normalized clustering coefficient (γ) (γ = Cp/Cprand, where Cp is the real clustering coefficients and Cprand is the same calculated from a matched random network) (30), normalized characteristic path length (λ) (λ = Lp/Lprand, where Lp is the real characteristic path length and Lprand is the same calculated from a matched random network) (30), the number of random networks selected in the calculation of the small word attribute is 100. The most parameter is the small worldness (σ, $\sigma = \gamma/\lambda$), a small-world network has similar path length but higher clustering than a random network, that means $\lambda>1$, $\lambda\approx1$; network efficiency parameters: global efficiency (Eg) and local efficiency (Eloc) (Eglob and Eloc are the measures of network efficiency in transmitting information at the local and global levels, respectively) (30); and nodal parameters: Ne, nodal local efficiency (Nloc), nodal clustering coefficient (NCp), degree centrality (Dc), and betweenness centrality (Bc). When brain graphs were constructed, each graph of the participants was thresholded to create an equal number of nodes and edges across them. We operated network parameters over a range of threshold values to guarantee high correlation coefficients of the remaining connections. The sparsity threshold, which denotes the ratio between

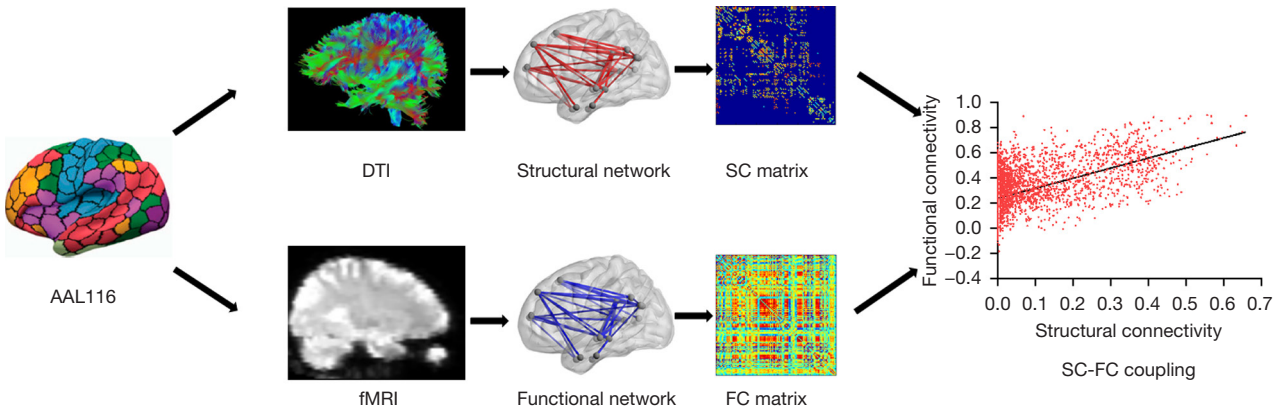

Figure 1 Flow chart of data analysis. SC matrix and FC matrix is computed from fMRI and DTI respectively based on the AAL116 atlas. FC-SC coupling strength is calculated as the correlation between FC and SC matrices. DTI, diffusion tensor imaging; fMRI, functional magnetic resonance imaging; SC, structural connectivity; FC, functional connectivity; AAL, automated anatomical labeling.

the number of actual edges and to all the possible edges in the matrix was applied to create the binary network (23). In the study, a sparsity threshold ranging from 0.05 to 0.5 with an interval of 0.01 was chosen to remove the possible false edges. Furthermore, the area under the curve (AUC) over the full range of defined sparsity thresholds was calculated for each network topological metric. The AUC provides a summarized scale for the topologic characterization of brain networks and is sensitive to topologic alterations in brain disorders (31).

Functional-structural coupling

The analysis of FC-SC coupling was described in previous studies (8,18,19,32,33). We calculated Pearson's correlation coefficients between the functional and structural network matrix, which is considered the network coupling strength, for each participant (*Figure 1*). The analysis was performed at the group and individual levels (32). At the group level, the mean FC and mean SC matrix were computed as the average of the FC and SC matrices of all participants within each group. The nonzero network edges of the SC matrix were extracted, rescaled to Gaussian distribution, and correlated with their functional counterparts to develop one FC-SC correlation coefficient for each group. Negative connections were discarded because the number was small. At the individual level, a single FC-SC "coupling" value was calculated as the correlation between the strength of the non-zero SC edges and corresponding FC within each participant.

Statistical analysis

Statistical analysis of demographic and neuropsychological data was performed using SPSS software 20.0 (SPSS, Chicago, IL, United States). Differences in demographic information and neuropsychological measures between the mTBI group and the HC group were analyzed using independent two-sample t-tests for normal distribution (age, education level, and MoCA score) and Mann-Whitney U tests for non-normal distribution (MoCA-VEIS, MoCA-NIS, MoCA-AtIS, MoCA-AbIS, MoCA-OIS, MoCA-MIS, and MoCA-LIS). A Chi-square test was applied for group differences in sex.

Group differences in FC and SC global and nodal properties (AUC values for network topologic parameters) were examined by a two-sample *t*-test (age, sex, and education level as covariates) with Bonferroni corrections for multiple comparisons in MATLAB. Group differences in FC-SC correlation coefficients at the group level were compared using Fisher's z test. FC-SC coupling between two groups at the individual level was compared using general linear models controlling for age, sex, and education level with Bonferroni corrections for multiple comparisons. Data for group differences are presented as the means, standard deviations, P values and Cohen's d statistic for effect sizes.

After significant intergroup differences were identified in the network measures, Spearman's rank correlations were computed between these measures and the neuropsychological test scores in the total group of patients with acute mTBI using MATLAB (34). The potential

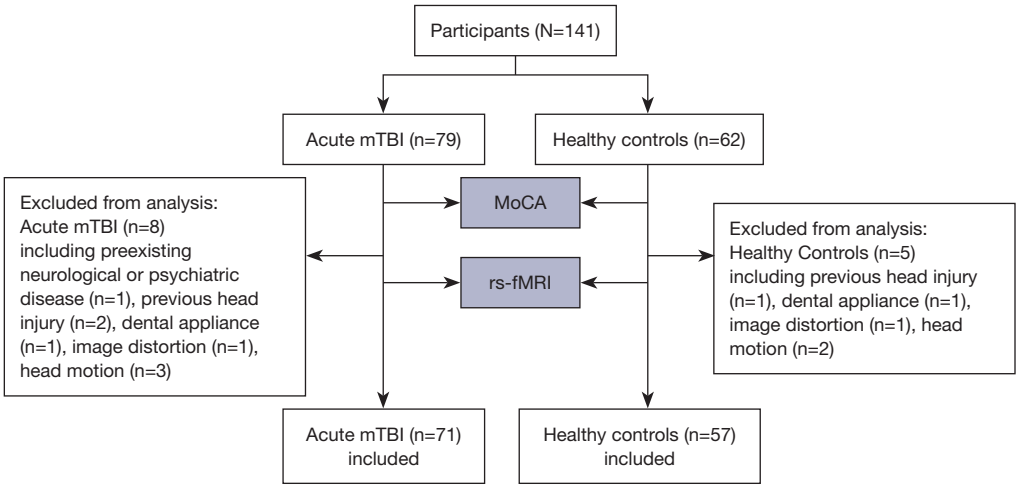

Figure 2 Flow chart of the participants enrollment. mTBI, mild traumatic brain injury; MoCA, Montreal Cognitive Assessment; rs-fMRI, Resting-state functional magnetic resonance imaging.

confounding factors including age, sex, and education level, motion and time post-injury were set as nuisance covariates in the analysis. Correction for multiple comparisons was performed using Bonferroni corrections. P<0.05 was considered statistically significant.

Results

Demographic and neuropsychological data

During the study period, 221 patients who presented to our emergency department were diagnosed with acute mTBI. Among them, 109 (49.3%) patients with acute mTBI were contacted and 79 (72.5%) of 109 were willing to participate in our study. Among the 79 patients with acute mTBI, 8 (10.1%) were excluded. Among the total 62 HC, 5 (8%) were excluded. The number and the reason were showed in *Figure 2*. Thus, the data from the remaining 71 patients within an average of 3.29 days (range, 0–10 days) after head injury and 57 HC were finally analyzed. *Table 1* lists the basic comparison of demographic characteristics of 71 acute mTBI patients versus 57 HC. Both groups did not show any significant difference in age (P=0.13, d=–0.272), sex (P=0.05), or years of education (P=0.14, d=–0.270). The mTBI group had lower MoCA, MoCA-VEIS and MoCA-AbIS scores than the HC group (P<0.001, d=–0.864; P=0.002, d=–0.747; P=0.001, d=–0.824). There were no significant differences between groups with respect to MoCA-NIS, MoCA-AtIS, MoCA-MIS, MoCA-LIS and MoCA-OIS (P=0.44, d=0.105; P=0.16, d=–0.401; P=0.47, d=–0.110; P=0.73, d=–0.076; P=0.09, d=–0.421). All participants showed no abnormalities on CT or MRI (FLAIR and SWI).

Aberrant global FC and SC network

The mTBI group and HC group demonstrated an economical small word organization (γ>1 and λ=1) of FC networks constructed at all connection densities (0.05–0.5) following the AAL-116 parcellation scheme. Patients with acute mTBI showed significantly increased γ in the functional network (*Figure 3A* and *Table 2*). The mTBI group and HC group also demonstrated an economical small world organization (γ>1 and $\lambda\approx$1) in SC networks constructed at all connection densities (0.05–0.5), following the AAL-116 parcellation scheme. Patients with acute mTBI showed significantly increased γ and σ in the structural network (*Figure 3B* and *Table 2*).

Aberrant regional FC and SC network

Compared with the HC group, the mTBI group showed increased nodal properties (nodal degree, Ne, and Nloc) in the left inferior frontal gyrus, orbital part (ORBinf.L), right superior frontal gyrus, medial orbital (ORBsupmed.R), right parahippocampal gyrus (PHG.R), left Heschl gyrus (HES.L), right superior frontal gyrus, orbital part (ORBsup.R), IFGtriang.R, left amygdala_L (AMYG.L), ANG.R, TPOsup.R, left temporal pole: middle temporal gyrus (TPOmid.L),

Table 1 Comparison of demographic characteristics of acute mTBI patients versus healthy controls

Characteristics	mTBI (n=71)	HC (n=57)	P value	Cohen's d
Age (year)	43.54±10.43	46.16±8.79	0.13	–0.272
Sex (male/female)	29/42	33/24	0.05	NA
Education (year)	11.46±3.95	12.39±2.85	0.14	–0.270
GCS Score	15	NA	NA	NA
Time since injury (day)	3.29±2.30	NA	NA	NA
MoCA	24.00±3.07	26.30±2.18	<0.001*	–0.864
MoCA-VEIS	3.51±1.25	4.28±0.75	0.002*	–0.747
MoCA-NIS	2.87±0.38	2.83±0.38	0.44	0.105
MoCA-AtIS	5.34±0.95	5.66±0.61	0.16	–0.401
MoCA-LIS	2.23±0.66	2.28±0.65	0.73	–0.076
MoCA-AbIS	1.62±0.57	1.97±0.19	0.001*	–0.824
MoCA-MIS	2.55±1.26	2.72±1.79	0.47	–0.110
MoCA-OIS	5.73±0.48	5.90±0.31	0.09	–0.421

Data are presented as mean ± standard deviation. * denotes significant difference compared to HC, P<0.05. mTBI, mild traumatic brain injury; HC, healthy controls; GCS, Glasgow Coma Scale; MoCA, Montreal Cognitive Assessment; MoCA-VEIS, visual-executive index score; MoCA-NIS, naming index score; MoCA-AtIS, attention index score; MoCA-LIS, language index score; MoCA-AbIS, abstraction index score; MoCA-MIS, memory index score; MoCA-OIS, orientation index score; NA, not applicable.

and TPOmid.R (*Figure 4A* and Table S1). The mTBI group also exhibited decreased nodal properties in the left fusiform gyrus (FFG.L), left supramarginal gyrus (SMG.L), right cerebellum, vermis, left superior frontal gyrus, dorsolateral (SFGdor.L), right superior frontal gyrus, dorsolateral (SFGdor.R), right lingual gyrus (LING.R), and right inferior occipital gyrus (IOG.R) (*Figure 4A* and Table S1).

Compared with the HC group, the mTBI group showed increased nodal properties (nodal degree, nodal betweenness, NCp and Ne) in the right temporal pole: superior temporal gyrus (TPOsup.R), right inferior frontal gyrus, opercular part (IFGoperc.R), right supplementary motor area (SMA.R), left angular gyrus (ANG.L), right angular gyrus (ANG.R), and bilateral cerebellum (*Figure 4B* and Table S2). The mTBI group also had decreased nodal properties in the left hippocampus (HIP.L), vermis, left caudate nucleus (CAU.L), right lenticular nucleus, putamen (PUT.R), right precentral gyrus (PreCG.R), left middle temporal gyrus (MTG.L), left inferior frontal gyrus, opercular part (IFGoperc.L), right inferior frontal gyrus, triangular part (IFGtriang.R), right rolandic operculum (ROL.R), SMA.R, left superior frontal gyrus, medial (SFGmed.L), right insula (INS.R), right superior occipital gyrus (SOG.R), left middle occipital gyrus (MOG.L), ANG.L, right temporal pole: middle temporal gyrus (TPOmid.R), right inferior temporal gyrus (ITG.R), and right cerebellum (*Figure 4B* and Table S2).

Aberrant functional-structural coupling

At the group level, group-averaged FC was closely associated with group-averaged SC across all structurally defined connections within each group (mTBI: r=0.479, HC participants: r=0.451, P=0.08) (*Figure 5A,5B*). At the individual level, patients with acute mTBI had significantly higher FC-SC coupling than HC participants (0.218±0.039 *vs.* 0.203±0.033, P=0.02, d=0.415) (*Figure 5C* and *Table 2*). Thus, patients with acute mTBI showed a higher SC-FC correlation than HC participants.

Associations between FC, SC parameters, and FC-SC coupling and cognition

For the FC network, γ was negatively correlated with MoCA-OIS (rho =–0.274, P=0.01). Nodal degree and Ne of the ORBsupmed.R were negatively correlated with MoCA-OIS (rho =–0.274, P=0.02; rho =–0.259, P=0.02). Nloc of the LING.R was positively correlated with MoCA-NIS (rho

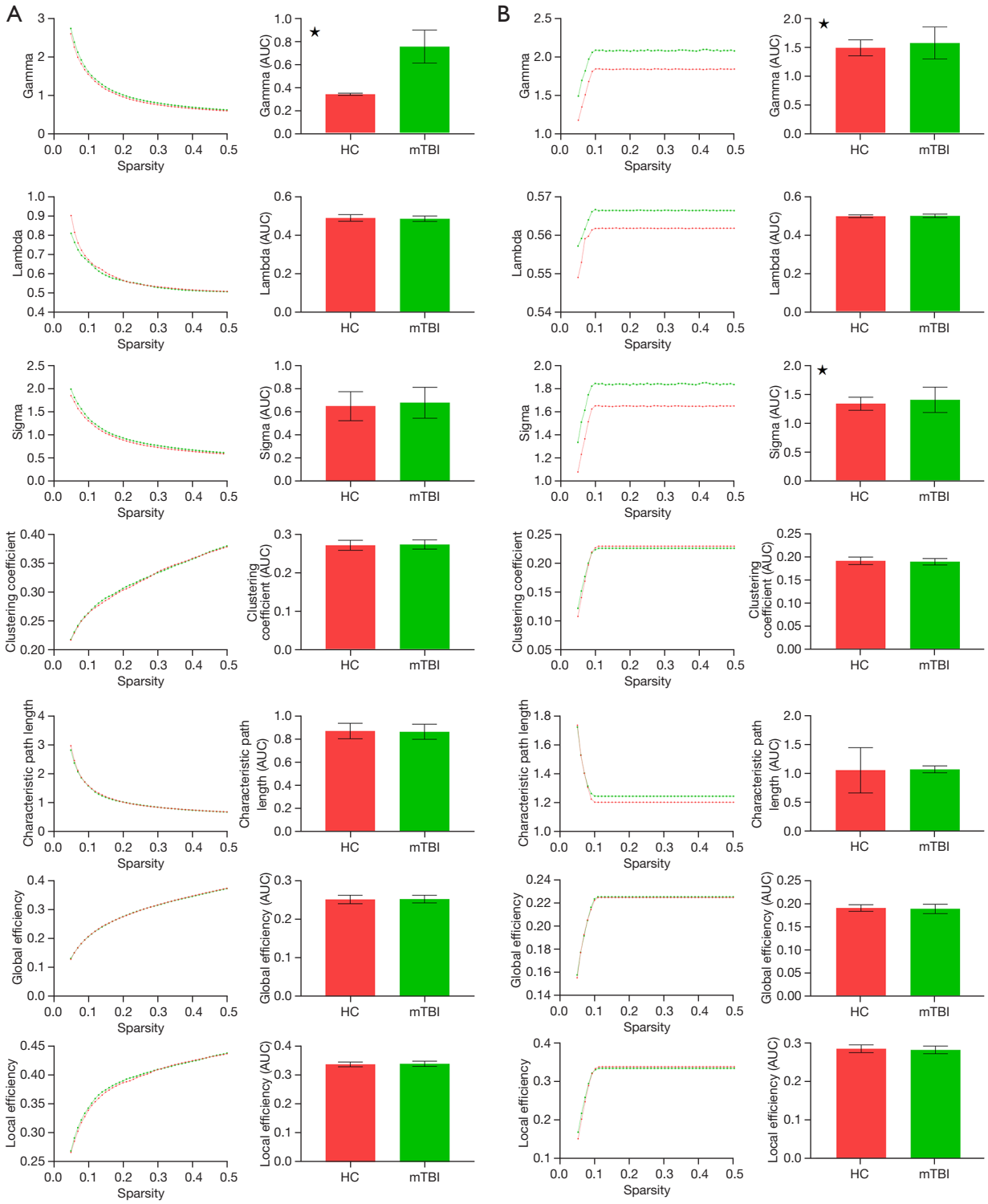

Figure 3 Global topology organization of the healthy controls (red) and mTBI (green). (A) Functional network measures of the global topology organization of the HCs and mTBI. (B) Structural network measures of the global topology organization of the HCs and mTBI. * denotes significant group differences. HC, healthy control; mTBI, mild traumatic brain injury; AUC, area under the curve.

Table 2 Brain network graph measures in acute mTBI patients and healthy controls

Graph measures	mTBI (n=71)	HC (n=57)	P value	Cohen's d
Functional network				
Gamma	0.75±0.14	0.34±0.01	<0.001*	4.076
Lambda	0.49±0.01	0.49±0.02	0.14	−0.257
Sigma	0.68±0.13	0.65±0.13	0.19	0.231
Cp	0.27±0.01	0.27±0.01	0.42	0.160
Lp	0.86±0.07	0.87±0.07	0.59	−0.091
Eg	0.26±0.01	0.25±0.01	0.75	0.095
Eloc	0.34±0.01	0.34±0.01	0.35	0.235
Structural network				
Gamma	1.57±0.28	1.48±0.14	0.03*	0.390
Lambda	0.50±0.01	0.50±0.01	0.14	0.248
Sigma	1.41±0.22	1.34±0.11	0.03*	0.395
Cp	0.19±0.01	0.19±0.01	0.11	−0.266
Lp	1.07±0.06	1.06±0.39	0.10	0.053
Eg	0.19±0.01	0.19±0.01	0.13	−0.232
Eloc	0.28±0.01	0.29±0.01	0.09	−0.300
Functional-structural coupling				
Coupling	0.22±0.04	0.20±0.03	0.02*	0.415

Data are presented as mean ± standard deviation. The AUC across the full range of sparsity thresholds was calculated for graph measures of functional and structural network. * denotes significant difference compared to HC, Bonferroni-corrected P<0.05. mTBI, mild traumatic brain injury; HC, healthy controls; Cp, clustering coefficient; Lp, characteristic path length; Eg, global efficiency; Eloc, local efficiency; AUC, area under the curve.

=0.340, P=0.004). Nloc of the IFGtriang.R was negatively correlated with MoCA-OIS (rho =−0.317, P=0.007). Nloc of the SFGdor.R was associated with MoCA-MIS (rho =−0.311, P=0.008). No correlations were found between SC-FC coupling parameters and MoCA scores (Table S3).

For the SC network, patients with acute mTBI showed a significant positive correlation between γ and σ and MoCA score (rho =0.267, P=0.02; rho =0.268, P=0.02, respectively), a significant positive correlation between γ and σ and MoCA-AtIS (rho =0.358, P=0.002; rho =0.324, P=0.006, respectively), a significant positive correlation between nodal degree of the HIP.L and MoCA-AIS (rho =0.287, P=0.01), a significant positive correlation between the nodal betweenness of the OLF.L and MoCA-AtIS (rho =0.293, P=0.01), and a significant positive correlation between the Ne of the SFGmed.L and MoCA-AtIS (rho =0.387, P=0.001) (Table S4).

Discussion

For the mTBI group, the functional and structural brain networks preserved small world characteristics. The γ and σ of the structural network and the γ of the functional network were significantly greater in patients with acute mTBI. An increase in γ was also reported in children with acute mTBI (12). These findings may reflect the compensatory response of the brain during the acute stage expecting that less impairment for those with larger network differences. The reason may be explained that brain regions are more connected at the local level across the entire network. Caeyenberghs *et al.* (35) found that adults with moderate to severe TBI showed increased γ during the 4-year follow-up, suggesting that the increase in γ would extend to persist longer following more severe TBI. In theory, the change in γ can result in the change in σ. In the present study, σ significantly increased in the structural network in acute mTBI. Similarly, Yuan *et al.* (12) found elevated σ at the acute stage. High levels of γ and σ in mTBI implied lower efficiency in global integration and a higher degree in regional segregation in their brain networks, reflecting a new balance between the competing demands for wiring cost and resilience to pathological conditions (12). However, this study failed to find changes in σ of the functional network, suggesting that structural connection alterations exert more effect on acute mTBI. Wang *et al.* (20) found no significant changes in σ in the acute stage possibly due to differences in sample size, AAL parcellation scheme without considering the importance of cerebellum, and sparsity threshold value. Further investigation with a larger number of participants and consistent parameters is needed to clarify whether changes in σ will be found in acute mTBI.

In addition to global functional and structural outcomes, aberrant nodal topology of FC and SC networks was found in patients with acute mTBI. Although the difference between functional and structural networks is small, our findings demonstrate evidence of functional and structural abnormalities mainly in the frontal, temporal, cerebellum, and subcortical areas, which are associated with mTBI. Reduced neural activity was also found in the frontal lobe, including the inferior frontal gyrus, middle frontal gyrus, and superior frontal gyrus, in mTBI (36). The temporal

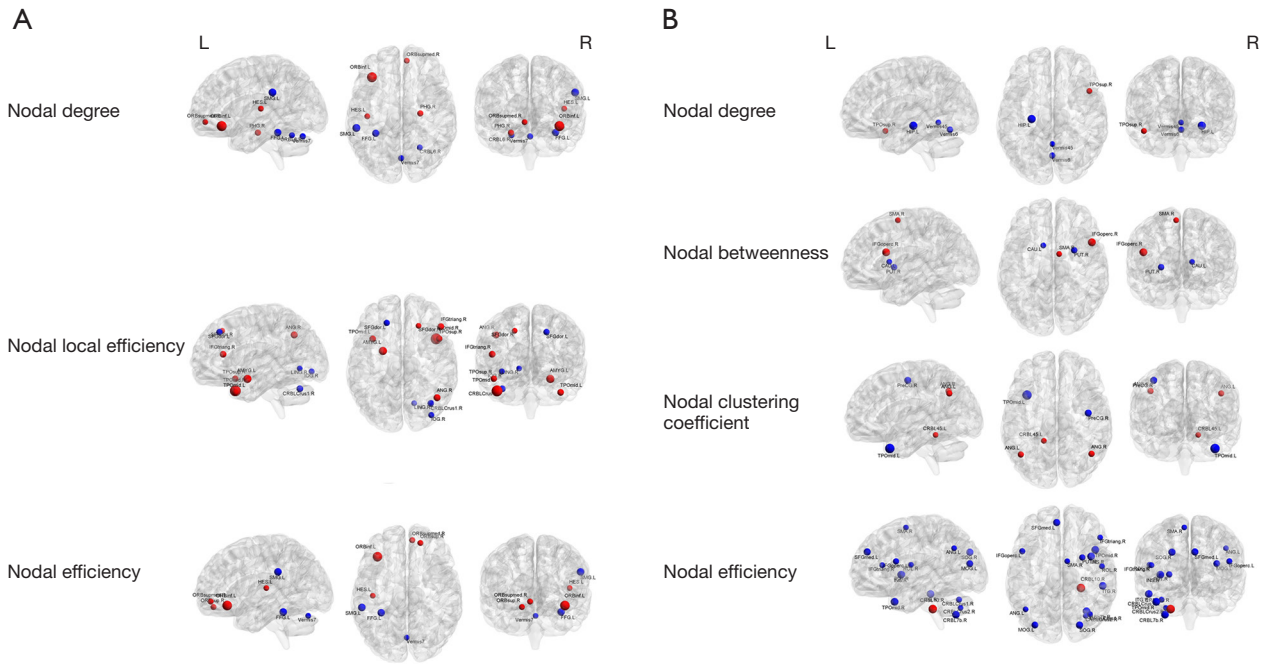

Figure 4 Regional organization of all participants. (A) Functionally, regions showing decreased and increased nodal centralities in acute mTBI patients compared with healthy controls, including nodal degree, nodal local efficiency and nodal efficiency. (B) Structurally, regions showing decreased and increased nodal centralities in acute mTBI patients compared with healthy controls, including nodal degree, nodal betweenness, nodal clustering coefficient and nodal efficiency. Correction for multiple comparisons was performed using Bonferroni method ($P<0.05$). L, left; R, right; mTBI, mild traumatic brain injury.

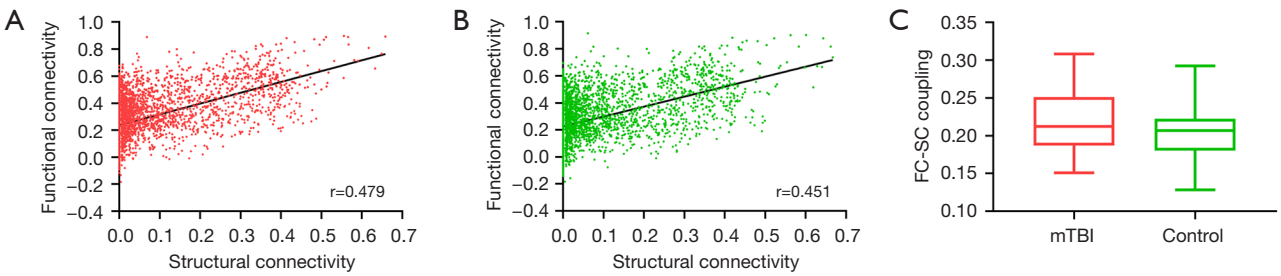

Figure 5 Functional-structural connectivity coupling at both the group-level and the individual level. (A) Functional-structural connectivity coupling of the mTBI at the group-level. (B) Functional-structural connectivity coupling of healthy controls at the group-level (C) Functional-structural connectivity coupling of the mTBI and healthy control participants at the individual-level. FC, functional connectivity; SC, structural connectivity; mTBI, mild traumatic brain injury.

lobe, which is located at the midline, is vulnerable to brain injury. FC aberrances of the temporal lobe were found in the mTBI group in previous literature. At the acute stage, cerebral blood flow was reduced in the frontal lobe, occipital lobe, and parietal lobe (37). The frontal and subcortical gray regions also presented subtle lesions on SWI (38). To date, emerging evidence has demonstrated the involvement of cerebellum in mTBI (39). Patients with mTBI during the acute phase exhibited abnormal fractional anisotropy of the cerebellum region (39). Differences in frontal, temporal, cerebellum, and subcortical nodes may reflect reduced cortex integration, indicating the reduced role of the certain hubs in global network information processing with acute mTBI. The increased nodal centralities observed in the

study indicate a possible compensatory mechanism for decreased connectivity.

FC-SC coupling can be altered under physiological and pathological states (40-42). This study is the first to demonstrate FC-SC coupling in acute mTBI at the group and individual levels. As predicted, the FC-SC relationship was aberrant in patients with acute mTBI. Our study found increased FC-SC coupling compared with HC in agreement with previous studies that reported increased coupling in schizophrenia, epilepsy, anesthesia, and kidney transplantation (8,42-44). This phenomenon could be explained by the fact that patients with mTBI experience the most dramatic change in the acute phase because FC fluctuates in a complex pattern, reflecting a wealth of potential dynamics. As mentioned above, however, no correlation was found between FC-SC coupling and cognitive tests. Thus, the reliable relationship between FC–SC coupling and cognitive decline remains to be evaluated in future work.

Weak correlations were found between functional and structural network properties and neuropsychological test scores in patients with acute mTBI. Orientation, attention, naming, and memory were preferentially affected among patients with acute mTBI. In our study, the alterations of global and nodal FC properties were more likely to affect orientation function, and the alterations of global and nodal SC properties were found to be more correlated with attention. The correlated nodes were mainly distributed in the frontal lobe, followed by the temporal lobe. These findings are supported by previous studies that reported cognitive impairments in the mTBI population at the acute stage (36,45,46). The present findings also suggest a theoretical model in which the frontal lobe is an essential integrating node in brain networks to control high-order cognitive function. In humans, frontal lobe functions are conditional on the development of an intricate set of short- and long-range connections that guarantee direct access to most aspects of cognition and behavior or control over regions dedicated to cognitive information processing (47).

Several limitations of this study need to be addressed. First, the sample size was small; despite the clear findings, the replication of the study in a larger cohort is mandatory. Second, although this study aimed to examine cognitive impairment following mTBI at the acute stage, imaging data were only acquired once within 14 days following brain injury. No longitudinal data were available at additional time points for studying the progression of recovery. Thus, further prospective studies are warranted. Third, many brain areas have been verified to have complex fiber architecture including crossing fibers. DTI acquisition and deterministic tractography approaches are limited to distinguishing crossing fibers. In future studies, advanced tractography approaches based on neurite orientation dispersion and density imaging (NODDI) data may help to provide more accurate anatomical connectivity patterns of brain networks.

Conclusions

Our study revealed brain network damage with regard to functional and structural large-scale networks and SC-FC coupling strength in mTBI patients, compared with HC. These damages were related to cognitive impairment following acute mTBI. Our findings provide an implicative neural basis for the alterations of large-scale brain networks and valuable information to elucidate the neuropathological mechanisms of cognitive impairment after mTBI in the acute phase.

Acknowledgments

Funding: This work was funded by the Natural Science Foundation of China (Nos. 82102012 and 82102006).

Footnote

Reporting Checklist: The authors have completed the STROBE reporting checklist. Available at https://qims.amegroups.com/article/view/10.21037/qims-22-450/rc

Conflicts of Interest: All authors have completed the ICMJE uniform disclosure form (available at https://qims.amegroups.com/article/view/10.21037/qims-22-450/coif). The authors have no conflicts of interest to declare.

Ethical Statement: The authors are accountable for all aspects of the work in ensuring that questions related to the accuracy or integrity of any part of the work are appropriately investigated and resolved. The study was conducted in accordance with the Declaration of Helsinki (as revised in 2013). The study was approved by the Institutional Review Board of Nanjing Medical University. Written informed consent was obtained from all participants before their participation in the study protocol.

References

1. Forcione M, Yakoub KM, Chiarelli AM, Perpetuini D, Merla A, Sun R, Sawosz P, Belli A, Davies DJ. Dynamic contrast-enhanced near-infrared spectroscopy using indocyanine green on moderate and severe traumatic brain injury: a prospective observational study. Quant Imaging Med Surg 2020;10:2085-97.
2. Maas AIR, Menon DK, Adelson PD, Andelic N, Bell MJ, Belli A, et al. Traumatic brain injury: integrated approaches to improve prevention, clinical care, and research. Lancet Neurol 2017;16:987-1048.
3. Carroll EL, Outtrim JG, Forsyth F, Manktelow AE, Hutchinson PJA, Tenovuo O, Posti JP, Wilson L, Sahakian BJ, Menon DK, Newcombe VFJ. Mild traumatic brain injury recovery: a growth curve modelling analysis over 2 years. J Neurol 2020;267:3223-34.
4. Samuelson KW, Engle K, Abadjian L, Jordan J, Bartel A, Talbot M, Powers T, Bryan L, Benight C. Cognitive Training for Mild Traumatic Brain Injury and Posttraumatic Stress Disorder. Front Neurol 2020;11:569005.
5. Huang S, Huang C, Li M, Zhang H, Liu J. White Matter Abnormalities and Cognitive Deficit After Mild Traumatic Brain Injury: Comparing DTI, DKI, and NODDI. Front Neurol 2022;13:803066.
6. Schneider ALC, Huie JR, Boscardin WJ, Nelson L, Barber JK, Yaffe K, Diaz-Arrastia R, Ferguson AR, Kramer J, Jain S, Temkin N, Yuh E, Manley GT, Gardner RC; TRACK-TBI Investigators. Cognitive Outcome 1 Year After Mild Traumatic Brain Injury: Results From the TRACK-TBI Study. Neurology 2022;98:e1248-61.
7. Li L, Yerra L, Chang B, Mathur V, Nguyen A, Luo J. Acute and late administration of colony stimulating factor 1 attenuates chronic cognitive impairment following mild traumatic brain injury in mice. Brain Behav Immun 2021;94:274-88.
8. Zhang Z, Liao W, Chen H, Mantini D, Ding JR, Xu Q, Wang Z, Yuan C, Chen G, Jiao Q, Lu G. Altered functional-structural coupling of large-scale brain networks in idiopathic generalized epilepsy. Brain 2011;134:2912-28.
9. Chen H, Geng W, Shang S, Shi M, Zhou L, Jiang L, Wang P, Yin X, Chen YC. Alterations of brain network topology and structural connectivity-functional connectivity coupling in capsular versus pontine stroke. Eur J Neurol 2021;28:1967-76.
10. Zarkali A, McColgan P, Leyland LA, Lees AJ, Rees G, Weil RS. Organisational and neuromodulatory underpinnings of structural-functional connectivity decoupling in patients with Parkinson's disease. Commun Biol 2021;4:86.
11. Cao R, Wang X, Gao Y, Li T, Zhang H, Hussain W, Xie Y, Wang J, Wang B, Xiang J. Abnormal Anatomical Rich-Club Organization and Structural-Functional Coupling in Mild Cognitive Impairment and Alzheimer's Disease. Front Neurol 2020;11:53.
12. Yuan W, Wade SL, Babcock L. Structural connectivity abnormality in children with acute mild traumatic brain injury using graph theoretical analysis. Hum Brain Mapp 2015;36:779-92.
13. Han K, Mac Donald CL, Johnson AM, Barnes Y, Wierzechowski L, Zonies D, Oh J, Flaherty S, Fang R, Raichle ME, Brody DL. Disrupted modular organization of resting-state cortical functional connectivity in U.S. military personnel following concussive 'mild' blast-related traumatic brain injury. Neuroimage 2014;84:76-96.
14. Zhou Y. Small world properties changes in mild traumatic brain injury. J Magn Reson Imaging 2017;46:518-27.
15. van der Horn HJ, Liemburg EJ, Scheenen ME, de Koning ME, Spikman JM, van der Naalt J. Graph Analysis of Functional Brain Networks in Patients with Mild Traumatic Brain Injury. PLoS One 2017;12:e0171031.
16. Greicius MD, Supekar K, Menon V, Dougherty RF. Resting-state functional connectivity reflects structural connectivity in the default mode network. Cereb Cortex 2009;19:72-8.
17. Sporns O. The human connectome: a complex network. Ann N Y Acad Sci 2011;1224:109-25.
18. Jiang H, Zhu R, Tian S, Wang H, Chen Z, Wang X, Shao J, Qin J, Shi J, Liu H, Chen Y, Yao Z, Lu Q. Structural-functional decoupling predicts suicide attempts in bipolar disorder patients with a current major depressive episode. Neuropsychopharmacology 2020;45:1735-42.
19. Wang YF, Gu P, Zhang J, Qi R, de Veer M, Zheng G, Xu Q, Liu Y, Lu GM, Zhang LJ. Deteriorated functional and structural brain networks and normally appearing

functional-structural coupling in diabetic kidney disease: a graph theory-based magnetic resonance imaging study. Eur Radiol 2019;29:5577-89.
20. Wang S, Gan S, Yang X, Li T, Xiong F, Jia X, Sun Y, Liu J, Zhang M, Bai L. Decoupling of Structural and Functional Connectivity in Hubs and Cognitive Impairment After Mild Traumatic Brain Injury. Brain Connect 2021;11:745-58.
21. Li MJ, Huang SH, Huang CX, Liu J. Morphometric changes in the cortex following acute mild traumatic brain injury. Neural Regen Res 2022;17:587-93.
22. Eskridge SL, Macera CA, Galarneau MR, Holbrook TL, Woodruff SI, MacGregor AJ, Morton DJ, Shaffer RA. Influence of combat blast-related mild traumatic brain injury acute symptoms on mental health and service discharge outcomes. J Neurotrauma 2013;30:1391-7.
23. Ponsford J, Carrier S, Hicks A, McKay A. Assessment and Management of Patients in the Acute Stages of Recovery after Traumatic Brain Injury in Adults: A Worldwide Survey. J Neurotrauma 2021;38:1060-7.
24. Frenette LC, Tinawi S, Correa JA, et al. Early detection of cognitive impairments with the Montreal Cognitive Assessment in patients with uncomplicated and complicated mild traumatic brain injury. Brain Inj 2018. [Epub ahead of print]. doi: 10.1080/02699052.2018.1542506.
25. Prajapati R, Emerson IA. Global and regional connectivity analysis of resting-state function MRI brain images using graph theory in Parkinson's disease. Int J Neurosci 2021;131:105-15.
26. Li F, Liu Y, Lu L, Shang S, Chen H, Haidari NA, Wang P, Yin X, Chen YC. Rich-club reorganization of functional brain networks in acute mild traumatic brain injury with cognitive impairment. Quant Imaging Med Surg 2022;12:3932-46.
27. Cui Z, Zhong S, Xu P, He Y, Gong G. PANDA: a pipeline toolbox for analyzing brain diffusion images. Front Hum Neurosci 2013;7:42.
28. Mori S, Crain BJ, Chacko VP, van Zijl PC. Three-dimensional tracking of axonal projections in the brain by magnetic resonance imaging. Ann Neurol 1999;45:265-9.
29. Wang J, Wang X, Xia M, Liao X, Evans A, He Y. GRETNA: a graph theoretical network analysis toolbox for imaging connectomics. Front Hum Neurosci 2015;9:386.
30. Benito-León J, Sanz-Morales E, Melero H, Louis ED, Romero JP, Rocon E, Malpica N. Graph theory analysis of resting-state functional magnetic resonance imaging in essential tremor. Hum Brain Mapp 2019;40:4686-702.
31. Li Z, Chen R, Guan M, Wang E, Qian T, Zhao C, Zou Z, Beck T, Shi D, Wang M, Zhang H, Li Y. Disrupted brain network topology in chronic insomnia disorder: A resting-state fMRI study. Neuroimage Clin 2018;18:178-85.
32. Wang J, Khosrowabadi R, Ng KK, Hong Z, Chong JSX, Wang Y, Chen CY, Hilal S, Venketasubramanian N, Wong TY, Chen CL, Ikram MK, Zhou J. Alterations in Brain Network Topology and Structural-Functional Connectome Coupling Relate to Cognitive Impairment. Front Aging Neurosci 2018;10:404.
33. Zhang D, Zhu P, Yin B, Zhao P, Wang S, Ye L, Bai L, Yan Z, Bai G. Frontal White Matter Hyperintensities Effect on Default Mode Network Connectivity in Acute Mild Traumatic Brain Injury. Front Aging Neurosci 2022;13:793491.
34. van der Horn HJ, Kok JG, de Koning ME, Scheenen ME, Leemans A, Spikman JM, van der Naalt J. Altered Wiring of the Human Structural Connectome in Adults with Mild Traumatic Brain Injury. J Neurotrauma 2017;34:1035-44.
35. Caeyenberghs K, Leemans A, Leunissen I, Gooijers J, Michiels K, Sunaert S, Swinnen SP. Altered structural networks and executive deficits in traumatic brain injury patients. Brain Struct Funct 2014;219:193-209.
36. Lu L, Li F, Ma Y, Chen H, Wang P, Peng M, Chen YC, Yin X. Functional connectivity disruption of the substantia nigra associated with cognitive impairment in acute mild traumatic brain injury. Eur J Radiol 2019;114:69-75.
37. Peng SP, Li YN, Liu J, Wang ZY, Zhang ZS, Zhou SK, Tao FX, Zhang ZX. Pulsed arterial spin labeling effectively and dynamically observes changes in cerebral blood flow after mild traumatic brain injury. Neural Regen Res 2016;11:257-61.
38. Spitz G, Maller JJ, Ng A, O'Sullivan R, Ferris NJ, Ponsford JL. Detecting lesions after traumatic brain injury using susceptibility weighted imaging: a comparison with fluid-attenuated inversion recovery and correlation with clinical outcome. J Neurotrauma 2013;30:2038-50.
39. Wang Z, Wu W, Liu Y, Wang T, Chen X, Zhang J, Zhou G, Chen R. Altered Cerebellar White Matter Integrity in Patients with Mild Traumatic Brain Injury in the Acute Stage. PLoS One 2016;11:e0151489.
40. Honey CJ, Sporns O, Cammoun L, Gigandet X, Thiran JP, Meuli R, Hagmann P. Predicting human resting-state functional connectivity from structural connectivity. Proc Natl Acad Sci U S A 2009;106:2035-40.
41. Hagmann P, Sporns O, Madan N, Cammoun L, Pienaar R, Wedeen VJ, Meuli R, Thiran JP, Grant PE. White

matter maturation reshapes structural connectivity in the late developing human brain. Proc Natl Acad Sci U S A 2010;107:19067-72.
42. Skudlarski P, Jagannathan K, Anderson K, Stevens MC, Calhoun VD, Skudlarska BA, Pearlson G. Brain connectivity is not only lower but different in schizophrenia: a combined anatomical and functional approach. Biol Psychiatry 2010;68:61-9.
43. Cocchi L, Harding IH, Lord A, Pantelis C, Yucel M, Zalesky A. Disruption of structure-function coupling in the schizophrenia connectome. Neuroimage Clin 2014;4:779-87.
44. Chen HJ, Wang YF, Wen J, Xu Q, Lu GM, Zhang LJ. Functional-structural relationship in large-scale brain networks of patients with end stage renal disease after kidney transplantation: A longitudinal study. Hum Brain Mapp 2020;41:328-41.
45. Sampedro F, Marín-Lahoz J, Martínez-Horta S, Pagonabarraga J, Kulisevsky J. Reduced gray matter volume in cognitively preserved COMT 158Val/Val Parkinson's disease patients and its association with cognitive decline. Brain Imaging Behav 2020;14:321-8.
46. Jilka SR, Scott G, Ham T, Pickering A, Bonnelle V, Braga RM, Leech R, Sharp DJ. Damage to the Salience Network and interactions with the Default Mode Network. J Neurosci 2014;34:10798-807.
47. Catani M. The anatomy of the human frontal lobe. Handb Clin Neurol 2019;163:95-122.

Cite this article as: Liu Y, Li F, Shang S, Wang P, Yin X, Krishnan Muthaiah VP, Lu L, Chen YC. Functional-structural large-scale brain networks are correlated with neurocognitive impairment in acute mild traumatic brain injury. Quant Imaging Med Surg 2023;13(2):631-644. doi: 10.21037/qims-22-450

Supplementary

Table S1 Brain regions showing increased and decreased nodal properties of functional network in acute mTBI patients compared with healthy controls

Brain region	t value	P value
Increased nodal properties		
Nodal degree		
Frontal_Inf_Orb_L	3.4910	<0.001
Frontal_Mid_Orb_R	2.0232	0.04
ParaHippocampal_R	2.1899	0.03
Heschl_L	2.0559	0.04
Nodal efficiency		
Frontal_Sup_Orb_R	2.0726	0.04
Frontal_Inf_Orb_L	3.3794	<0.001
Frontal_Mid_Orb_R	2.0716	0.04
Heschl_L	1.9920	0.04
Nodal local efficiency		
Frontal_Inf_Tri_R	2.3630	0.01
Amygdala_L	2.8748	0.004
Angular_R	2.4615	0.01
Temporal_Pole_Sup_R	2.2469	0.02
Temporal_Pole_Mid_L	2.3394	0.02
Temporal_Pole_Mid_R	3.8232	<0.001
Decreased nodal properties		
Nodal degree		
Fusiform_L	–2.5671	0.01
SupraMarginal_L	–2.7595	0.006
Cerebellum_Superior_R	–2.1193	0.03
Vermis7	–2.1859	0.03
Nodal efficiency		
Fusiform_L	–2.6484	0.009
SupraMarginal_L	–2.6768	0.008
Vermis 7	–2.0148	0.04
Nodal local efficiency		
Frontal_Sup_L	–2.2212	0.02
Frontal_Sup_R	–1.9848	0.04
Lingual_R	–2.0078	0.04
Occipital_Inf_R	–2.1218	0.03
Cerebellum_Superior_R	–2.3575	0.01

The P values are obtained by using the Bonferroni corrections. R, right; L, left; Frontal_Inf_Orb, Inferior frontal gyrus, orbital part; Frontal_Mid_Orb, Middle frontal gyrus, orbital part; Frontal_Sup_Orb, Superior frontal gyrus, orbital part; Frontal_Inf_Tri, Inferior frontal gyrus, triangular part; Temporal_Pole_Sup, Temporal pole: superior temporal gyrus; Temporal_Pole_Mid, Temporal pole: middle temporal gyrus; Frontal_Sup, Superior frontal gyrus, dorsolateral; Occipital_Inf, Inferior occipital gyrus.

https://dx.doi.org/10.21037/qims-22-450

Table S2 Brain regions showing increased and decreased nodal properties of structural network in acute mTBI patients compared with healthy controls

Brain region	t value	P value
Increased nodal properties		
Nodal degree		
Temporal_Pole_Sup_R	2.0557	0.04
Nodal betweenness		
Frontal_Inf_Oper_R	2.7623	0.006
Supp_Motor_Area_R	2.0269	0.04
Nodal clustering coefficient		
Angular_L	2.1706	0.03
Angular_R	2.2151	0.02
Cerebellum_Superior_L	2.0023	0.04
Nodal efficiency		
Cerebellum_Inferior_R	3.0034	0.003
Decreased nodal properties		
Nodal degree		
Hippocampus_L	−2.8850	0.004
Vermis 4	−2.0132	0.04
Vermis 6	−2.2443	0.02
Nodal betweenness		
Caudate_L	−2.0073	0.04
Putamen_R	−2.2520	0.02
Nodal clustering coefficient		
Precentral_R	−2.4766	0.01
Temporal_Mid_L	−3.2954	0.001
Nodal efficiency		
Frontal_Inf_Oper_L	2.1760	0.03
Frontal_Inf_Tri_R	2.0446	0.04
Rolandic_Oper_R	2.0402	0.04
Supp_Motor_Area_R	1.9878	0.04
Frontal_Sup_Medial_L	2.5113	0.01
Insula_R	2.71887	0.007
Occipital_Sup_R	2.5686	0.01
Occipital_Mid_L	2.4049	0.01
Angular_L	1.9918	0.04
Putamen_R	2.2121	0.02
Temporal_Pole_Mid_R	2.7392	0.007
Temporal_Inf_R	2.6811	0.008
Cerebellum_Superior_R	2.1098	0.03
Cerebellum_Inferior_R	1.9839	0.0494
Cerebellum_Inferior_R	2.7049	0.007

The P values are obtained by using the Bonferroni corrections. R, right; L, left; Temporal_Pole_Sup, Temporal pole: superior temporal gyrus; Frontal_Inf_Oper, Inferior frontal gyrus, opercular part; Temporal_Mid, Middle temporal gyrus; Frontal_Inf_Tri, Inferior frontal gyrus, triangular part; Rolandic_Oper, Rolandic operculum; Frontal_Sup_Medial, Superior frontal gyrus, medial; Occipital_Sup, Superior occipital gyrus; Occipital_Mid, Middle occipital gyrus; Temporal_Pole_Mid, Temporal pole: middle temporal gyrus; Temporal_Inf, Inferior temporal gyrus.

https://dx.doi.org/10.21037/qims-22-450

Table S3 Correlations between global and nodal properties of functional network and MoCA in mTBI patients

FC properties	MoCA-NIS	MoCA-OIS	MoCA-MIS
Gamma	–	rho=−0.274, P=0.01	–
Nodal degree	–	rho=−0.274, P=0.02(ORBsupmed.R)	–
Nodal efficiency	–	rho=−0.259, P=0.02(ORBsupmed.R)	–
Nodal local efficiency	rho=0.340, P=0.004(LING.R)	rho=−0.317, P=0.007((IFGtriang.R)	rho=−0.311, P=0.008(SFGdor.R)

The P values are obtained by using the Bonferroni corrections. mTBI, mild traumatic brain injury; FC, functional connectivity; MoCA, Montreal Cognitive Assessment; MoCA-NIS, naming index score; MoCA-OIS, orientation index score; MoCA-MIS, memory index score; R, right; ORBsupmed, Superior frontal gyrus, medial orbital; LING, Lingual gyrus; IFGtriang, Inferior frontal gyrus, triangular part; SFGdor, Superior frontal gyrus, dorsolateral.

Table S4 Correlations between global and nodal properties of structural network and MoCA in mTBI patients

SC properties	MoCA score	MoCA-AIS
Gamma	rho=0.267, P=0.02	rho=0.358, P=0.002
Sigma	rho=0.268, P=0.02	rho=0.324, P=0.006
Nodal degree	–	rho=0.287, P=0.01(HIP.L)
Nodal betweenness	–	rho=0.293, P=0.01(OLF.L)
Nodal efficiency	–	rho=0.387, P=0.001(SFGmed.L)

The P values are obtained by using the Bonferroni corrections. mTBI, mild traumatic brain injury; SC, structural connectivity; MoCA, Montreal Cognitive Assessment; MoCA-AtIS, attention index score; L, left; HIP, Hippocampus; OLF, Olfactory cortex; SFGmed, Superior frontal gyrus, medial.

https://dx.doi.org/10.21037/qims-22-450